This is the accepted version of the following article:

Martin Motola, Hanna Sopha, Miloš Krbal, Luděk Hromádko, Zuzana Olmrová Zmrhalová, Gustav Plesch, Jan M. Macak (2018). Comparison of photoelectrochemical performance of anodic single- and double-walled TiO2 nanotube layers. *Electrochemistry Communications.* doi.org/10.1016/j.elecom.2018.09.015

This postprint version is available from URI: https://hdl.handle.net/10195/71824

Publisher's version is available from

https://www.sciencedirect.com/science/article/pii/S1388248118302509

This postprint version is licenced under a Creative Commons Attribution-NonCommercial-NoDerivatives 4.0.International.

Comparison of Photoelectrochemical Performance of Anodic Single- and Double-Walled TiO_2 Nanotube Layers

Martin Motola[1,2], Hanna Sopha[1,3], Miloš Krbal[1], Luděk Hromádko[1], Zuzana Olmrová Zmrhalová[1], Gustav Plesch[2], Jan M. Macak[1,3*]

[1]*Center of Materials and Nanotechnologies, Faculty of Chemical Technology, University of Pardubice, Nam.Čs.Legii 565, 53002 Pardubice, Czech Republic*
[2]*Department of Inorganic Chemistry, Faculty of Natural Sciences, Comenius University, Ilkovičova 6, Mlynská Dolina, 842 15 Bratislava, Slovak Republic*
[3] *Central European Institute of Technology, Brno University of Technology, Purkyňova 123, 612 00 Brno, Czech Republic*

*Corresponding author: e-mail address: jan.macak@upce.cz (J.M. Macak)

ABSTRACT

In this work, the photoelectrochemical response of single-walled (SW) and double-walled (DW) TiO_2 nanotube (TNT) layers is presented. TNT layers were grown on Ti substrates by anodization in two different ethylene glycol-based electrolytes to obtain ~5 and ~15 µm thick TNT layers. The inner shell of the TNT was quantitatively removed *via* a mild pre-annealing followed by a selective chemical etching treatment in piranha solution. All TNT layers were investigated for their photoelectrochemical response in the ultraviolet and near visible spectral range. Significantly enhanced photocurrent densities were revealed for the SW-TNT layers. This is ascribed to improved charge carrier separation along the tube walls due to the lack of the C- and F-rich inner shell removed by etching.

Keywords: titanium dioxide, nanotubes, single-walled, double-walled, photoelectrochemistry

1. Introduction

Over the past two decades, self-organized anodic TiO_2 nanotube (TNT) layers have been intensively investigated for a wide range of applications [1-7]. From the photoelectrochemical view, TNT layers represent one of the most interesting and promising TiO_2 nanostructures [8-10]. TNT layers in particular possess unidirectional charge transport, strong light absorption owing to its conical shape, high surface area and the ability to suppress the recombination of photoexcited charge carriers [10-12].

TNT layers are grown directly on the Ti surface by anodization [13,14] in suitable electrolytes containing HF or fluoride salts. Several nanotube generations have been developed, based on anodization in aqueous HF electrolytes [15,16], aqueous NaF or NH_4F electrolytes [17,18], or organic-based electrolytes [19-23]. In the meantime, there is a good understanding of the influence of anodization conditions, substrates, and electrolytes on the resulting nanotube layers and their dimensions, spacing and ordering [24-31]. Nowadays, ethylene glycol-based electrolytes with NH_4F and water are the most used electrolytes [14,25]. However, in these electrolytes a double layer oxide is formed, as first shown by Albu et al. [32]. The double layer is composed of an inner (IS) and an outer (OS) shell, yielding the double-walled (DW) structure.

As reported by Liu et al. [33], the origin of the DW can be explained considering the nanotube formation mechanism. During the anodization, TiO_2 is formed on two distinct places, on the metal – metal oxide interface and on the metal oxide – electrolyte interface. Thereby, the oxide formed on the metal oxide – electrolyte interface contains carbon species due to the contamination from the adsorbed electrolyte species. Whereas the oxide formed on the metal - metal oxide interface consists of TiO_2 with significantly lower C content. Considering the plastic flow model [33,34] for the nanotube formation, the pure TiO_2 layer builds the OS of the nanotubes and the C-containing oxide builds the IS. Recently, deep investigations were carried out studying the exact composition of the OS and IS [35,36]. The results show clearly a high C contamination of the IS, originating from the voltage induced decomposition of the electrolyte, as well as a contamination with F species. All in all, the IS can be considered as significantly C-rich and F-rich compared to the OS.

Several recent papers from the Schmuki´s group report on the removal of the IS and positive impact of the single-walled (SW) nanotubular structure on the efficiency of dye-sensitized solar cells [33, 37-39]. From these papers it becomes clear that the IS affects the morphology and properties of TNT layers. However, there is a large room to explore the SW TNT layers further, since the SW structure may increase the performance of TNT layers in various applications (e.g. photocatalysis, batteries, capacitors, etc.), as the carbon containing IS have negative contribution to the charge recombination [33].

To the best of our knowledge, there is no study about the comparison of the photoelectrochemical properties of SW and DW TNT layers of different aspect ratio. Therefore, the preparation of two types of SW TNT layers from classical self-organized DW TNT layers is demonstrated in this work using mild pre-annealing and chemical treatment in piranha solution to dissolve the IS. The influence of the IS on photoelectrochemical performance of nanotube layers is investigated against reference DW TNT layers.

2. Experimental

Two types of TiO_2 nanotube (TNT) layers were used in this work: ~5µm and ~15µm thick layers. They were prepared *via* electrochemical anodization using previously published recipes at 100 V [40] and 60 V [41] in fluoride containing ethylene glycol-based electrolyte. They possess an average inner diameter of ~230 nm and ~135 nm, respectively.

In order to remove the IS that consists of a C- and F-rich TiO_2, a selective chemical treatment reported by the Schmuki´s group [38, 39] was used and optimized for the TNT layers presented in this paper. First, the prepared TNT layers were pre-annealed at 135 °C and 150 °C for 5µm and 15µm tubes, respectively, for 1 hour in air using a heating rate of 15 °C/min. Second, the layers were immersed in piranha solution (H_2SO_4:H_2O_2 = 3:1; LachNer, Czech Republic) for 10 min (5µm tubes) and 8 min (15µm tubes), respectively, at 70 °C. After etching, the layers were immersed in H_2O and EtOH for 1 min, respectively, and dried with a nitrogen jet, yielding single-walled TNT layers, indicated as SW TNT. In order to obtain the anatase structure, the nanotubes were subsequently annealed in air in a muffle oven (400 °C, 1 h). A part of the nanotube layers (indicated as DW TNT layers in this work) was kept for reference without any chemical treatment but annealed in the same way.

A field-emission scanning electron microscope (FE-SEM, JEOL JSM 7500F) was used for morphological characterization. The morphological parameters of TNT layers were evaluated by statistical analyses of SEM images using proprietary Nanomeasure software.

Thermogravimetric analyses (TGA) were carried out under air atmosphere (20 ml/min, Linde) using a PerkinElmer Pyris 1 TGA with high temperature furnace. Each sample (≈ 10 mg of weight) was placed in a Pt pan with ceramic liner and heated from laboratory temperature to 1000 °C in four successive steps: heating to 400° C (2.3 °C/min), holding for 60 min, heating to 1000 °C (10 °C/min), and holding for 60 min.

The photocurrent measurements of TNT layers were carried out in an aqueous 0.1 M Na_2SO_4 at 0.4 $V_{vs.Ag/AgCl}$ in the spectral range from 300 to 420 nm. A photoelectric spectrophotometer (Instytut Fotonowy) with a 150 W Xe lamp and a monochromator with a bandwidth of 5 nm connected with the modular electrochemical system AUTOLAB (PGSTAT 204, MetrohmAutolab B.V., Nova 1.10 software) was the measuring setup. Photocurrent stability tests were carried out by measuring the photocurrent produced under chopped light irradiation (light/dark cycles of 10 s). The CV curves were recorded in an aqueous 0.1 M Na_2SO_4 by scanning from -0.4 V to 1 $V_{vs.Ag/AgCl}$ at a sweeping rate of 5 mV/s started at 0 V towards positive voltages in the dark and under UV irradiation (355 nm).

3. Results and Discussion

Fig. 1A and B shows top-view images of 5µm and 15µm thick TNT layers with diameter ~230 nm and ~135 nm, respectively. Due to the presence of the IS, the decrease in diameter to ~100 nm (Fig. 1C) and ~55 nm (Fig. 1D) at the bottom of the TNT layer is revealed, respectively. It is necessary to point out that the thickness of the IS strongly increases towards the nanotube bottom. The IS at the very top of the nanotubes is dissolved due to the etching by the anodization solution (into TiF_6^{2-} complexes), compared to the

nanotube bottom parts, resulting in a V-shaped profile of the nanotubes [32,33]. Besides that, the IS is mainly composed of C- and F-rich oxide or oxy-hydroxide [39] which may have some negative consequences on the nanotube properties. In contrast, the OS of TNT is composed mainly of TiO_2 [39]. The IS can be relatively easily dissolved with a controlled etching treatment, as described in the experimental section and in previous works [38,39]. The use of optimized temperature (70 °C) and etching time (10 min for 5µm; 8 min for 15µm TNT) leads to the IS removal, resulting in the increase of the inner diameter to about 190 nm and 105 nm for 5µm and 15µm TNT, respectively, at the very bottom of the tubes. This can be clearly seen from Fig. 1E and F, respectively. The thickness of the TNT layer remained unchanged during the etching, as shown in Fig. 1 G and H. However, prolonging the etching time and/or increasing the temperature over the optimized values results in the TNTs layers to peel off from the Ti substrates. For shorter time and/or lower temperatures, the IS is not completely dissolved.

Fig. 2 shows photocurrent densities and the incident photon-to-electron conversion efficiencies (IPCE) recorded for both 5µm and 15µm TNT layers in SW as well as DW morphology, in the wavelength range from 300 to 420 nm. As seen from Fig. 2A and B, for both 5µm and 15µm TNT, a pronounced increase of photocurrent densities can be observed for the SW TNT layer compared to their DW counterparts. The IPCE data (Fig. 2C and D) are in the agreement with the obtained photocurrent densities. The increase in photocurrent densities and IPCEs for SW TNT layers compared to DW ones can be ascribed to the removal of the C-rich and F-rich inner shell originating from the electrolyte during the anodization process [38,39]. However, a slight shift towards lower wavelengths for 15µm TNTs is obtained (see the onset of the photocurrent and IPCE in Fig. 2B and D). This might be explained by a significantly higher amount of the C-rich TiO_2 removed from 15µm TNT layers compared to the 5µm case. The presence of such amount of this C-rich TiO_2 within 15µm TNT layers before etching is responsible for the light absorption edge shifted to longer wavelengths. To verify this hypothesis, the C-content within TNT layers was analysed using TGA performed in air with the DW amorphous TNT layers of both thicknesses. Intentionally a very high end temperature (1000°C) was used to promote oxidation of carbonaceous species and their burn-out. An absolute weight loss of 12.7% and 16.2% was recorded for the 5 and 15 µm thick TNT layers, respectively, which clearly confirms higher overall amount of C in DW 15 µm thick TNT layers compared to the 5 µm thick ones.

For further analysis, photocurrent transients were recorded and examined in detail. Different wavelengths were used to demonstrate the improvement of photocurrent density and IPCE after etching of the IS. Namely, 300 nm representing the photoresponse in the „hard“ UV spectral range and 355 nm which corresponds to the photocurrent density maximum of SW. An unambiguous increase of photocurrent densities (at $\lambda = 300$ nm) from 7.6 µA/cm^2 to 9.8 µA/cm^2 and from 10 µA/cm^2 to 16 µA/cm^2 for SW 5µm and 15µm TNT layers can be seen from Fig. 2E and F, respectively. In addition, the photocurrent densities recorded at $\lambda = 355$ nm for SW 5µm and 15µm TNT layers, respectively, show an increase from 18.4 µA/cm^2 to 26.4 µA/cm^2 (Fig. 2G) and from 34.2 µA/cm^2 to 51.7 µA/cm^2 (Fig. 2H). Another feature apparent from Fig. 2E to H is that the photocurrent densities of DW TNT

layers show a delay in time response, when the light is turned ON/OFF. Similar features were observed in previous publications [8,9,42]. This can be ascribed to numerous electron traps in the DW TNT layers resulting in pronounced charge recombination. Oxygen vacancies in the TiO_2 structure are typically assigned to be responsible for this behavior [43, 44]. The kinetics of the delay (slower response for 300 nm then for 355 nm) shows wavelength dependence as well as SW/DW dependence, since SW TNT layers possess lower amount of electron traps. Additionally, also the distinct granular morphology of the carbon containing IS (visible in Fig. 1C and D) might have negative contribution to the charge recombination [33]. However, the carbon compounds are evaporated during the annealing as CO_2, causing voids in the structure [33]. Therefore, the unwanted charge recombination is significantly reduced for SW TNT layers with the removal of the IS, diminishing the photocurrent delays.

Fig. 3A-D represents cyclic voltammetry (CV) curves obtained for the SW and DW TNTs in the dark (solid line) and under UV irradiation (λ = 355 nm, dotted line). In general, the CV shape for both SW and DW TNTs is typical for the anatase structure [34]. As seen in Fig. 3, the dark currents are almost identical for both SW and DW TNT layers. After UV irradiation, the photocurrent densities are comparable for both SW and DW TNTs. The photocurrent densities for all samples increased until the potential of ~0.4 V. At higher potentials a photocurrent plateau was observed indicating that the thickness of the nanotube walls equals the space charge layer [8]. Guiding lines drawn at 0.4 V point out at differences in the recorded photocurrents among all types of samples shown, since this potential was used for photocurrent and IPCE measurement in Fig. 2. For SW TNTs, the photocurrents are in both cases higher than for DW TNTs, however, the difference is not as pronounced as in Fig. 2. This stems from the fact that the dynamics of the CV experiments compared to the IPCE measurements is very different as various aspects come into play here: light absorption at different wavelength, applied voltage, kinetics of electron-hole separation, electron transfer including speed of trap filling, etc. Thus, it is not easy to make a link between these types of measurements, which is an interesting point frequently overlooked in literature.

4. Conclusions

In this work, we demonstrated the feasibility to chemically dissolve the C-rich and F-rich inner oxide shell of 5µm and 15µm thick TNT layers, which is presented in nanotubes produced in ethylene glycol-based electrolytes. Optimized etching treatment in piranha solution led to the dissolution of the C- and F-containing inner shell with an increase in the inner diameter of the nanotubes and the consequent formation of SW nanotube morphology. As a result, the nanotube walls consisted only of the pure TiO_2 outer shell. Photoelectrochemical studies showed that SW TiO_2 nanotubes of both thicknesses possess enhanced photocurrent densities with improved charge carrier transport along the nanotube walls due to the lack of C- and F-rich inner shell. The results clearly show a very promising pathway towards more efficient photoelectrochemical devices based on the TiO_2 nanotubular structures, enabling to etch the inner shell from virtually any type of DW TNT layers (after necessary process optimization).

Acknowledgements

European Research Council (project nr. 638857), Ministry of Youth, Education and Sports of the Czech Republic (project nr. LM2015082, LQ1601, CZ.02.1.01/0.0/0.0/16_013/0001829) and Scientific Grant Agency of the Slovak Republic (project VEGA nr. 1/0276/15) are acknowledged for financial support of this work.

References

[1] J.M. Macak, H. Tsuchiya, A. Ghicov, P. Schmuki, Dye-sensitized anodic TiO_2 nanotubes, Electrochem. Commun. 7 (2005) 1133-1138.

[2] J.M. Macak, M. Zlamal, J. Krysa, P. Schmuki, Self-organized TiO_2 nanotube layers as highly efficient photocatalysts, Small 3 (2007) 300-304.

[3] X. Gao, J. Li, J. Baker, Y. Hou, D. Guan, J. Chen, C. Yuan, Enhanced photovoltaic performance of perovskite $CH_3NH_3PbI_3$ solar cells with freestanding TiO_2 nanotube array films, Chem. Commun. 50 (2014) 6368−6371.

[4] O.K. Varghese, D. Gong, M. Paulose, K.G. Ong, C.A. Grimes, Hydrogen sensing using titania nanotubes, Sensor. Actuator. B-Chem. 93 (2003) 338-344.

[5] N.A. Kyerematen, N. Plylahan, A.C.S. dos Santos, L. V. Taveira, L.F.P. Dick, T. Djenizian, Sulfidated TiO_2 nanotubes: A potential 3D cathode material for Li-ion batteries, Chem. Commun. 49 (2013) 4205-4207.

[6] M. Motola, L. Satrapinskyy, T. Roch, J. Subrt, J. Kupcik, M. Klementova, M. Jakubickova, F. Peterka, G. Plesch, Anatase TiO_2 nanotube arrays and titania films on titanium mesh for photocatalytic NO_x removal and water cleaning, Catal. Today 287 (2017) 59–64.

[7] L. Assaud, N. Brazeau, M.K.S. Barr, M. Hanbücken, S. Ntais, E.A. Baranova, L. Santinacci, Atomic layer deposition of Pd nanoparticles on TiO_2 nanotubes for ethanol electrooxidation: synthesis and electrochemical properties, ACS Appl. Mater. Interfaces 2015, 7, 24533−24542.

[8] R. Beranek, H. Tsuchiya, T. Sugishima, J.M. Macak, L. Taveira, S. Fujimoto, H. Kisch, P. Schmuki, Enhancement and limits of the photoelectrochemical response from anodic TiO_2 nanotubes, Appl. Phys. Lett. 87 (2005) 243114-1 – 243114-3.

[9] H. Tsuchiya, J.M. Macak, A. Ghicov, A.S. Rader, L. Taveira, P. Schmuki, Characterization of electronic properties of TiO_2 nanotube films, Corrosion Sci. 49 (2007) 203-210.

[10] D. Regonini, G. Chen, C. Leach, F.J. Clemens, Comparison of photoelectrochemical properties of TiO_2 nanotubes and sol-gel, Electrochim. Acta 213 (2016) 31-36.

[11] N. R. de Tacconi, C. R. Chenthamarakshan, G. Yogeeswaran, A. Watcharenwong, R. S. de Zoysa, N. A. Basit, K. Rajeshwar, Nanoporous TiO_2 and WO_3 Films by Anodization of Titanium and Tungsten Substrates: Influence of Process Variables on Morphology and Photoelectrochemical Response, J. Phys. Chem. B, 110 (2006) 25347–25355.

[12] L.K. Tsui, T. Homma, G. Zangari, Photocurrent conversion in anodized TiO_2 nanotube arrays: effect of the water content in anodizing solutions, J. Phys. Chem. C 117 (2013) 6979-6989.

[13] J.M. Macak, H. Tsuchiya, A. Ghicov, K. Yasuda, R. Hahn, S. Bauer, P. Schmuki, TiO_2 nanotubes: self-organized electrochemical formation, properties and applications, Curr. Opin. Solid St. M. 11 (2007) 3-18.

[14] K. Lee, A. Mazare, P. Schmuki, One-dimensional titanium dioxide nanomaterials: Nanotubes, Chem. Rev. 114 (2014) 9385-9454.

[15] M. Assefpour-Dezfuly, C. Vlachos, E.H. Andrews, Oxide morphology and adhesive bonding on titanium surfaces, J. Mater. Sci. 19 (1984) 3626-3639.

[16] R. Beranek, H. Hildebrand, P. Schmuki, Self-organized porous titanium oxide prepared in H_2SO_4/HFelectrolytes, Electrochem. Solid-State Lett. 6 (2003) B12-B14.

[17] J.M. Macak, K. Sirotna, P. Schmuki, Self-organized porous titanium oxide in Na_2SO_4/NaF electrolytes, Electrochim. Acta 50 (2005) 3679-3684.

[18] J.M. Macak, H. Tsuchiya, P. Schmuki, High-aspect-ratio TiO_2 nanotubes by anodization of titanium, Angew. Chem. Int. Ed. 44 (2005) 2100-2102.

[19] J.M. Macak, H. Tsuchiya, L. Taveira, S. Aldabergerova, P. Schmuki, Smooth anodic TiO_2 nanotubes, Angew. Chem. Int. Ed. 44 (2005) 7463-7465.

[20] K. Zhu, N.R. Neale, A. Miedaner, A.J. Frank, Enhanced charge-collection efficiencies and light scattering in dye-sensitized solar cells using oriented TiO_2 nanotubes arrays, Nano. Lett. 7 (2007) 67-74.

[21] N.R. de Tacconi, W. Chanmanee, K. Rajeshwar, J. Rochford, E. Galoppini, Photoelectrochemical Behavior of Polychelate Porphyrin Chromophores and Titanium Dioxide Nanotube Arrays for Dye-Sensitized Solar Cells, J. Phys. Chem. C 113 (2009) 2996–3006.

[22] S.P. Albu, A. Ghicov, J.M. Macak, P. Schmuki, 250 µm long anodic TiO_2 nanotubes with hexagonal self-ordering, Phys. Status Solidi 1 (2007) R65-R67.

[23] M. Paulose, K. Shankar, S. Yoriya, H.E. Prakasam, O.K. Varghese, G.K. Mor, T.A. Latempa, A. Fitzgerald, C.A. Grimes, Anodic growth of highly ordered TiO_2 nanotube arrays to 134 µm in length, J. Phys. Chem. B 110 (2006) 16179-16184.

[24] K. Kant, D. Losic, Self-ordering electrochemical synthesis of TiO_2 nanotube arrays: controlling the nanotube geometry and the growth rate, Int. J. Nanosci. 10 (2011) 55-58.

[25] H. Sopha, L. Hromadko, K. Nechvilova, Jan M. Macak, Effect of electrolyte age and potential changes on the morphology of TiO_2 nanotubes, J. Electroanal. Chem. 759 (2015) 122-128.

[26] S. Ozkan, A. Mazare, P. Schmuki, Critical parameters and factors in the formation of spaced TiO_2 nanotubes by self-organizing anodization, Electrochim. Acta 268 (2018) 435-447.

[27] T. Kondo, S. Nagao, T. Yanagishita, N.T. Nguyen, K. Lee, P. Schmuki, H. Masuda, Ideally ordered porous TiO_2 prepared by anodization of pretextured Ti by nanoimprinting process, Electrochem. Commun. 50 (2015) 73–76.

[28] H. Sopha, T. Samoril, E. Palesch, L. Hromadko, R. Zazpe, D. Skoda, M. Urbanek, S. Ng, J. Prikryl, J.M. Macak, Ideally hexagonally ordered TiO_2 nanotube arrays, Chem. Open 6 (2017) 480-483.

[29] A. Crawford, N. Chawla, Tailoring TiO_2 nanotube growth during anodicoxidation by crystallographic orientation of Ti, Scripta Mater. 60 (2009) 874–877.

[30] S. Leonardi, V. Russo, A.L. Bassi, F. Di Fonzo, T.M. Murray, H. Efstathiadis, A. Agnoli, J. Kunze-Liebhäuser, TiO_2 nanotubes: interdependence if substrate grain orientation and growth rate, ACS Appl. Mater. Interfaces 7 (2015)1 662–1668.

[31] N. Hu, Gao N, Y. Chen, M.J. Starink, Achieving homogeneous anodic TiO_2 nanotube layers through grain refinement of the titanium substrate, Mater. Des. 110 (2016) 346–353.

[32] S. P. Albu, A. Ghicov, S. Aldabergenova, P. Drechsel, D. LeClere, G.E. Thompson, J.M. Macak, P. Schmuki, Formation of double-walled TiO_2 nanotubes and robust anatase membranes, Adv. Mater. 20 (2008) 4135-4139.

[33] N. Liu, H. Mirabolghasemi, K. Lee, S.P. Albu, A. Tighineanu, M. Altomare, P. Schmuki, Anodic TiO_2 nanotubes: double walled vs single walled, Faraday Discuss. 164 (2013) 107-116.

[34] S. Berger, S.P. Albu, F. Schmidt-Stein, H. Hildebrand, P. Schmuki, J.S. Hammond, D.F. Paul, S. Reichlmaier, The origin for tubular growth of TiO_2 nanotubes: a fluoride rich layer between tube-walls, Surf. Sci. 605 (2011) L57-L60.

[35] S. Mohajernia, A. Mazare, I. Hwang, S. Gaiaschi, P. Chapon, H. Hildebrand, P. Schmuki, Depth elemental characterization of 1D self-aligned TiO_2 nanotubes using calibrated radio frequency glow discharge optical emission spectroscopy (GDOES), Appl. Surf. Sci. 442 (2018) 412-416.

[36] A. Dronov, I. Gavrilin, E. Kirilenko, D. Dronova, S. Gavrilov, Investigation of anodic TiO_2 nanotube composition with high spatial resolution AES and ToF SIMS, Appl. Surf. Sci. 434 (2018) 148-154.

[37] H. Mirabolghasemi, N. Liu, K. Lee, P Schmuki, Formation of ‘single walled’ TiO_2 nanotubes with significantly enhanced electronic properties for higher efficiency dye-sensitized solar cells, Chem. Commun 49 (2013) 2067-2069.

[38] S. So, I. Hwang, P. Schmuki, Hierarchical DSSC structures based on “single walled” TiO_2 nanotube arrays reach a back-side illumination solar light conversion efficiency of 8%, Energy Environ. Sci. 8 (2015) 849-854.

[39] S. So, F. Riboni, I. Hwang, D. Paul, J. Hammond, O. Tomanec, R. Zboril, D.R. Sadoway, P. Schmuki, The double-walled nature of TiO_2 nanotubes and formation of tube-in-tube structures – a characterization of different tube morphologies, Electrochim. Acta 231 (2017) 721-731.

[40] S. Das, H. Sopha, M. Krbal, R. Zazpe, V. Podzemná, J. Prikryl, J.M. Macak, Electrochemica infilling of $CuInSe_2$ within TiO_2 layers and their photoelectrochemical studies, ChemElectroChem 4 (2017) 495-499.

[41] R. Zazpe, M. Knaut, H. Sopha, L. Hromadko, M. Albert, J. Prikryl, V. Gartnerova, J. W. Bartha, J.M. Macak, Atomic layer deposition for coating for high aspect ratio TiO_2 nanotube layers, Langmuir 32 (2016) 10551-10558.

[42] A. Ghicov, H. Tsuchiya, J.M. Macak, P. Schmuki, Annealing effects on the photoresponse of TiO_2 nanotubes, Phys. Status Solidi 203 (2006) R28-R30.

[43] M. Krbal, J. Kucharik, H. Sopha, H. Nemec, J.M. Macak, Charge transport in anodic TiO_2 nanotubes studied by terahertz spectroscopy, Phys. Status Solidi Rapid Res. Lett. 10 (2016) 691–695.

[44] T. Dittrich, Porous TiO_2: electron transport and application to dye sensitized injection solar cells, Phys. Status Solidi A 182 (2000) 447-455.

Figure captions

Fig. 1. SEM images of the tube tops (A, B), double-walled structure depicted at the tube bottoms (C, D), single-walled structure depicted at the tube bottoms (E, F) and cross-sections (G, H) of 5µm and 15µm thick TNT layers, respectively.

Fig. 2. (A, B) Photocurrent densities; (C, D) IPCE values recorded for annealed single- and double-walled TiO_2 nanotubes under UV irradiation; (E-H) Photocurrent transients of single- and double-walled TiO_2 nanotube layers recorded for 10 s under monochromatic UV irradiation with wavelength of (E, F) $\lambda = 300$ nm (G, H) 355 nm for 5µm and 15µm, respectively. All data recorded at 0.4 V vs Ag/AgCl.

Fig. 3. (A-D) CV curves obtained for SW 5µm (A) and 15µm (B) thick TNT layers, DW 5µm (C) and 15µm (D) TNT layers in the dark (solid lines) and under UV irradiation ($\lambda = 360$ nm dotted line). Guiding lines at 0.4 V are intentionally drawn there to link the photocurrent values with Fig. 2.

Figure 1

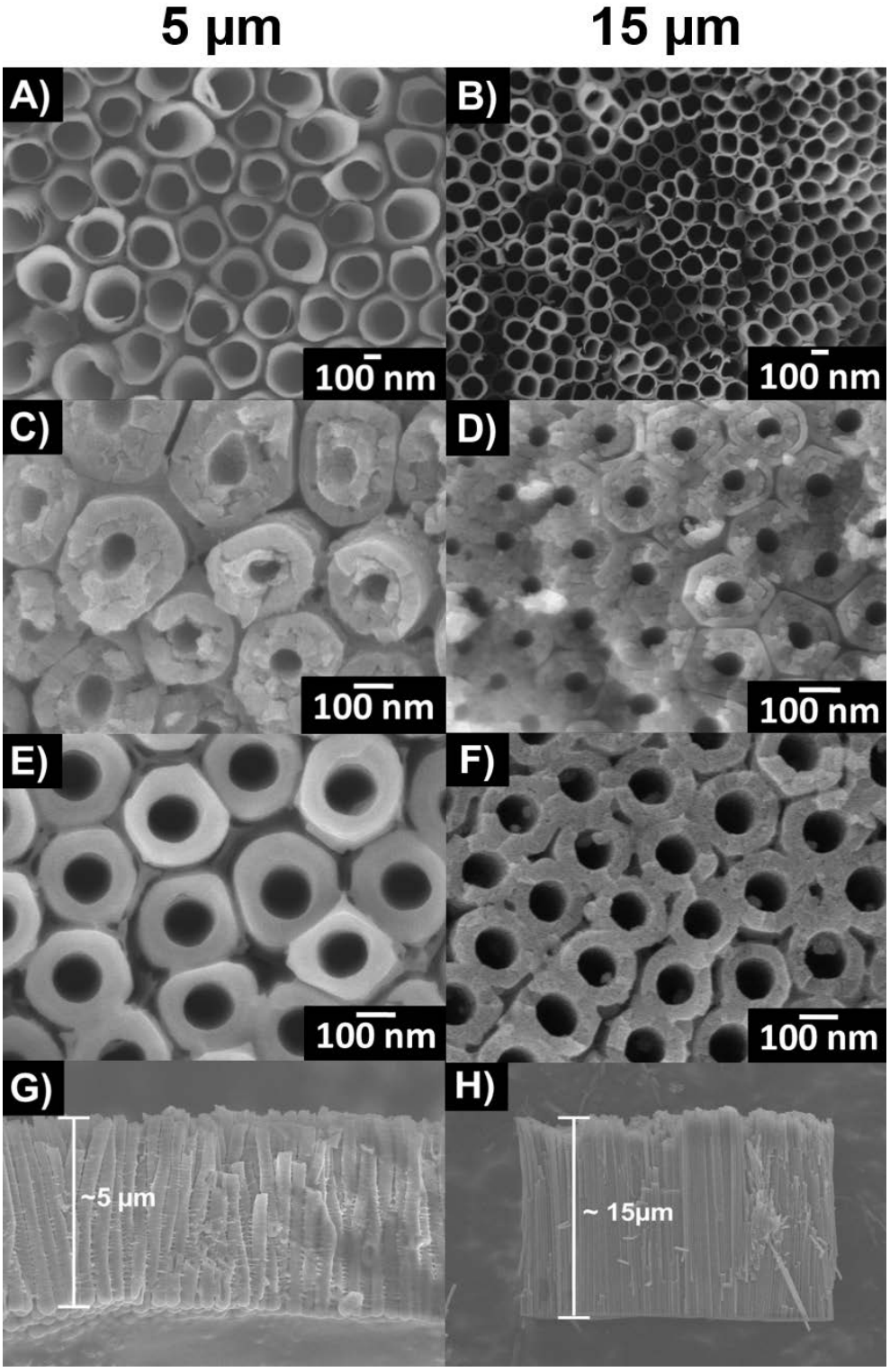

Figure 2

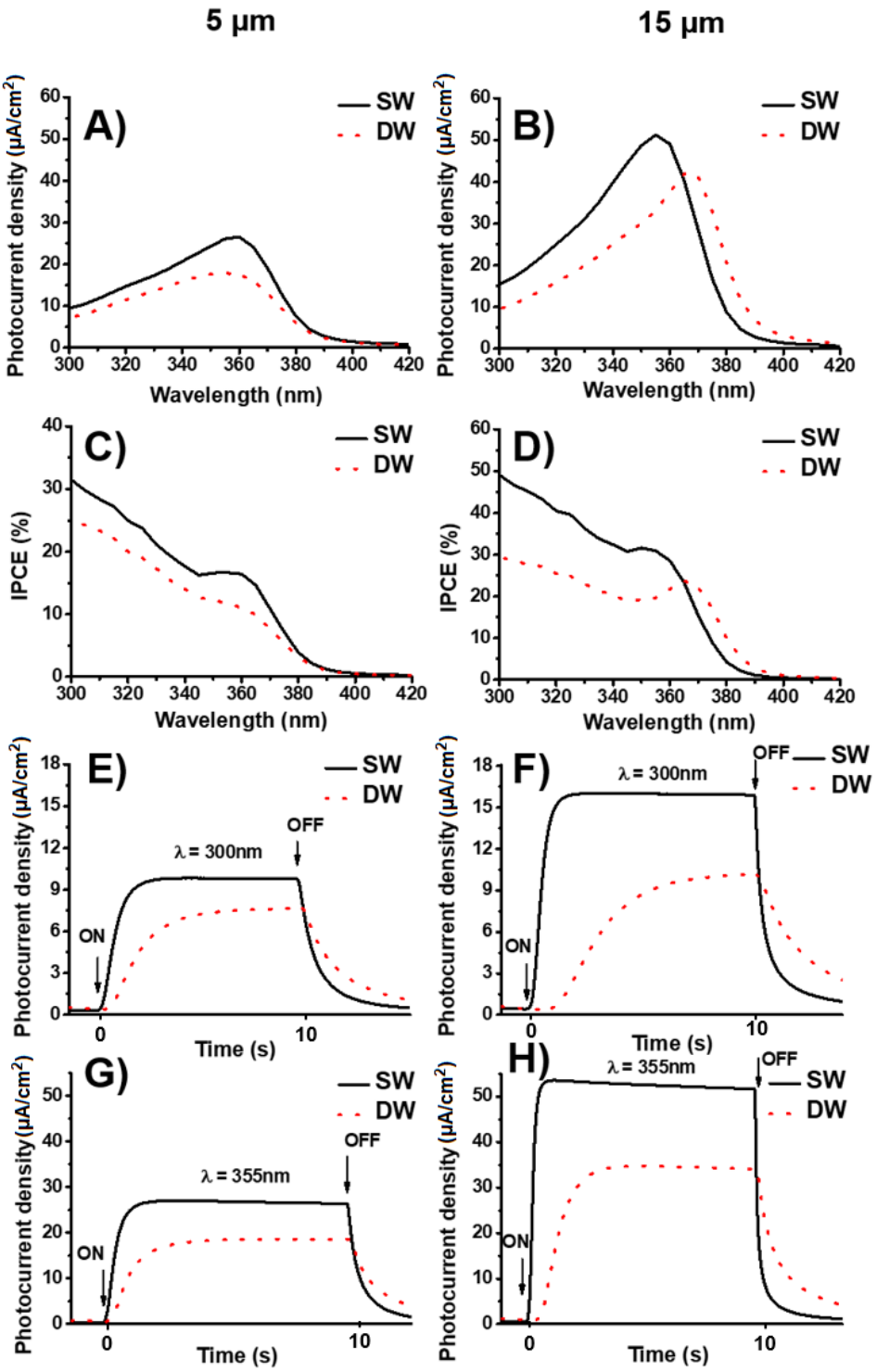
5 µm
15 µm
A)
B)
C)
D)
E)
F)
G)
H)
SW
DW
Photocurrent density (µA/cm²)
IPCE (%)
Wavelength (nm)
Time (s)
λ = 300nm
λ = 355nm
ON
OFF

Figure 3

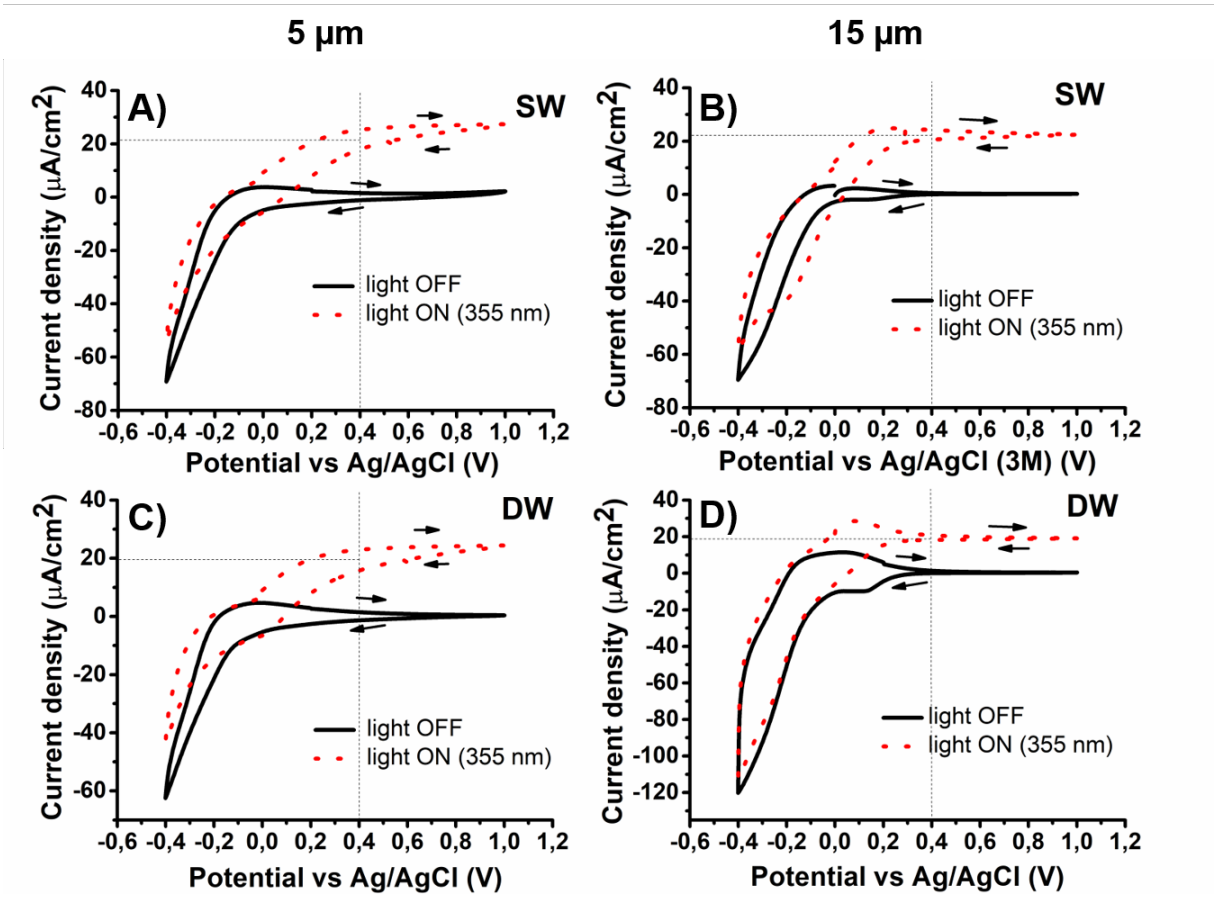
5 µm
15 µm
A)
SW
B)
SW
C)
DW
D)
DW
Current density (µA/cm2)
Potential vs Ag/AgCl (V)
Potential vs Ag/AgCl (3M) (V)
light OFF
light ON (355 nm)